Stability of interlanthanide perovskites ABO_3 ($A \equiv$ La-Pr; $B \equiv$ Y, Ho-Lu)

Cristina Artini [a, b,1], *Marcella Pani* [a, c], *Andrea Lausi* [d], *Giorgio A. Costa* [a, c]

[a] DCCI, Department of Chemistry and Industrial Chemistry, University of Genova, 16146 Genova, Italy

[b] CNR-IENI, 16149 Genova, Italy

[c] CNR-SPIN Genova, 16152 Genova, Italy

[d] Elettra - Sincrotrone Trieste S.C.p.A., 34149 Basovizza, Trieste, Italy

[1] corresponding author: artini@chimica.unige.it

Abstract

The existence fields of the eleven known interlanthanide perovskites have been assessed as a function of temperature on the basis of experimental and literature data, and studied by means of the bond valence method using the software SPuDS. The role of geometrical factors in driving the enthalpic and entropic contributions to the Gibbs free energy of the phase is discussed, and a criterion is proposed to derive the formability likelihood of interlanthanide perovskites. The reliability of the software SPuDS has been checked by comparing the cell parameters and atomic distances optimized by the program to the ones experimentally obtained by high temperature *in situ* synchrotron X-ray diffraction performed on perovskitic $LaErO_3$, $LaTmO_3$ and $LaYbO_3$.

Keywords: A. ceramics; A. oxides; C. X-ray diffraction; D. crystal structure; D. phase transitions.

1. Introduction

Interlanthanide perovskites form a small family of compounds studied for their remarkable properties as acceptor-doped protonic conductors [1,2,3,4], and high-k dielectrics [5,6]. They show also interesting magnetic properties [7,8,9], but despite their appealing features, fundamental studies on this topic are quite sporadic; only recently this and other research groups undertook investigations about synthesis, stability and structural peculiarities of these oxides [10,11,12,13].

A very large number of mixed oxides with general formula ABO_3, characterized by a wide variety of chemical and physical properties, crystallize in one of the perovskitic structural types; in the ideal case the cell is cubic and belongs to the $Pm\bar{3}m$ space group (isotypic crystal: $SrTiO_3$), with A in twelvefold and B in octahedral coordination towards oxygen. However, the great majority of perovskitic oxides presents a structural distortion consisting either in a cation displacement or in a tilting of the BO_6 octahedra; while the cation displacement only produces a distortion in the BO_6 polyhedra, the octahedral tilting has direct consequences on the lattice parameters, and for this reason it has been thoroughly investigated [14,15,16]; two different notations were introduced by Glazer [17] and Aleksandrov [18] to describe the octahedral tilting, that can be classified into 23 possible tilt systems belonging to 15 different space groups. Interlanthanide perovskites $LaREO_3$ (RE ≡ Y, Ho-Lu), $CeREO_3$ (RE ≡ Tm-Lu) and $PrREO_3$ (RE ≡ Yb-Lu) crystallize in the most common distorted perovskitic structure, namely the orthorhombic one, belonging to the *Pnma* space group (isotypic crystal: $GdFeO_3$), with atoms located in four atomic positions, namely La in 8*c* (*x*, ¼, *z*), RE in 4*b* (0, 0, 0), O1 in 8*d* (*x*, *y*, *z*) and O2 in 4*c* (*x*, ¼, *z*). According to the Glazer's notation, the structure belongs to the $a^+b^-b^-$ tilt system, meaning that the BO_6 octahedra are rotated by an angle *a* around the *x* axis and by an angle *b* around the *y* and *z* axes of the aristotype cubic coordinate system; signs indicate the in-phase (+) or out-of-phase (-) sense of rotation of neighbouring octahedra.

The closeness of a given perovskitic structure to the ideal cubic one is measured by the Goldschmidt tolerance factor *t* [19], a geometric agreement factor that accounts for the fitting of the A cation to the undistorted octahedral network. It is defined as

$$t = (R_A + R_O)/\sqrt{2}(R_B + R_O) \qquad (1)$$

where R_A, R_B and R_O are the Shannon's A, B and oxygen ionic radii [20]. The *t* range of the perovskitic structure has been determined by different authors during the last decades, and quite different results have been obtained. An old paper by Schneider and Roth [21] indicates 0.77-0.79 as the minimum *t* value necessary for the obtainment of a stable perovskite, while according to Randall et al. [22], the perovskitic structure is believed to exist for *t* ranging between 0.78 and 1.05, with values close to 1 corresponding to the undistorted cubic structure. Nevertheless, a more recent classification compiled by Zhang et al. [23] limits the formability of $A^{3+}B^{3+}O_3$ perovskites between 0.848 and 1.009; this *t* range appears to be more reasonable if data regarding interlanthanide perovskites are assessed: as discussed later, the minimum *t* value found for an interlanthanide perovskite is in fact 0.846 ($PrYbO_3$). Although 376 perovskitic and non-perovskitic ABO_3 oxides have been included in the aforementioned classification [23], only few interlanthanide perovskites are considered.

In undistorted perovskites the coordination of A and B towards oxygen is cubo-octahedral and octahedral, respectively; as in interlanthanide perovskites the A ion is too small with respect to B to ensure the stability of the ideal perovskite, the structure undergoes modifications which allow the A-centered cubo-octahedral site to better fit the A ionic radius. In all distorted perovskites the symmetry is lowered, and in the ones belonging to the *Pnma* space group, the lowering of symmetry is reached by the $a^+b^-b^-$ tilting of BO_6 octahedra, that causes a rearrangement in the position of oxygen atoms, with the consequent generation of two different atomic positions, namely the 8*d* (O1) and 4*c* (O2) sites.

Quite a large number of thermal and crystallographic high temperature studies [24,25,26,27,28,29,30] have been performed in the past on interlanthanide perovskites, showing the

presence of a certain solubility range of the perovskitic structure at high temperature. At the transition temperature they decompose into one of the structural forms typical of rare earth sesquioxides, namely either in the monoclinic (hereafter named B, space group *C*2/*m*, isotypic crystal: Sm_2O_3) or in one of the high temperature forms (H: hexagonal, X: cubic [31]); regarding the formation, they can directly derive from precursors, or from the cubic form typical of rare earth sesquioxides (hereafter named C, isotypic crystal: $(Mn_{0.5}Fe_{0.5})_2O_3$, space group: $Ia\bar{3}$). From the structural point of view, interlanthanide perovskitic oxides are characterized by a low value of the *t* factor, due to the small difference between A and B ionic radii; *t* ranges in fact between 0.8482 ($LaHoO_3$) and 0.8632 ($LaLuO_3$), locating these oxides close to the boundary of the perovskitic stability field. Considering the non existence of the perovskitic form of $LaDyO_3$ ($t = 0.8441$) and of other interlanthanide mixed oxides with $t \geq 0.82$, such as $CeREO_3$ (RE ≡ Dy-Er), $PrREO_3$ (RE ≡ Dy-Tm) and $NdREO_3$ (RE ≡ Dy-Yb) [8], as well as the doubtful existence of $NdLuO_3$, $LaHoO_3$ can be deemed as the end member of the series. It is well known that the prediction of phase stability in solid state chemistry is quite a difficult task, especially when it is based on theoretical models. On the contrary, when geometrical constraints prevail, it is mostly possible to derive a criterion able to predict the existence range of the studied phase. The perovskitic arrangement provides an example of a structure where the phase stability is ruled by the fitting degree of different polyhedra, concisely expressed by the Goldschmidt *t* factor. A recent work carried out by this research group showed that a correlation exists between *t* and the extent of the perovskitic stability field *vs.* temperature [10]; nevertheless, the only *t* factor is not sufficient to fully describe the structural variations with temperature, and more subtle geometrical factors affecting the enthalpic and entropic contribution to the Gibbs free energy of the phase have to be taken into consideration.

As a temperature-dependent stability criterion for interlanthanide perovskites has not been described so far, in the present work an approach based on the combined consideration of the Goldschmidt *t* factor and of RE-O bond distances calculated by the bond valence method at different temperatures, is proposed. By this approach it is possible to explain the correlation

between t and the extent of the perovskitic stability field, as well as the non-formability of several interlanthanide mixed oxides in the perovskitic form.

The bond valence method has been specifically applied to the study of perovskites by the program codes SPuDS and TUBERS [32], that allow to optimize the perovskitic structure by minimizing the difference between the formal valence and the calculated bond valence, and using composition and ionic oxidation states as the only input. An extensive work, carried out by Zhang *et al.* [23], was performed by using the cited software.

For the perovskites under investigation in the present work, located close to the phase boundary, interatomic distances and octahedral tilt angles were calculated by SPuDS. The reliability of the software in predicting structural features of interlanthanide perovskites was checked by comparing the experimental values of cell parameters and interatomic distances obtained from high temperature synchrotron X-ray diffraction results, as well as from literature data, to the values optimized at the same temperature by the program.

2. Experimental procedure

2.1 Sample synthesis

$LaREO_3$ (RE ≡ Er, Tm and Yb) samples were prepared by thermal treatment of the corresponding mixed oxalates at 873 K in air for one week. The treatment temperature was chosen with the aim to ensure the loss of all the CO_2 molecules from oxalates, and to obtain poorly crystalline oxides that could rearrange into the perovskitic form *in situ* just prior to the high temperature diffraction experiment. $(LaRE)_2[C_2O_4]_3{*}nH_2O$ mixed oxalates were synthesized by coprecipitation, as firstly described in [33,34]: stoichiometric amounts of La_2O_3 and RE_2O_3 (Alfa Aesar, 99.99%) were dissolved in HCl (13% wt.), and the two solutions were mixed together. A large excess of an oxalic acid solution was then added to the mixture, causing the precipitation of

the mixed oxalates, that were then filtered, washed with deionized water and dried in oven at 363 K overnight.

2.2 Synchrotron data collection

Mixed oxides obtained at 873 K were analyzed at the powder diffraction beamline (MCX) of the Elettra synchrotron radiation facility (Trieste, Italy), on a Huber 4-axis X-ray diffractometer equipped with a fast scintillator detector; making use of a Cyberstar hot-air blower, diffractograms were acquired at temperatures between 973 and 1273 K. Samples were placed in quartz capillary tubes (inner diameter: 0.5 mm) and rotated at a speed of 180 rpm; they were heated in air at 5K/min up to the desired temperatures: 973, 1073, 1173 and 1273 K, and maintained at each temperature for 2 hours prior to the acquisition of patterns. Diffractograms were collected for $8° \leq 2\theta \leq 55°$ with step 0.005°. The incident beam energy has been chosen at 18 keV, since this value is a good compromise between the requirements of the high energy necessary to minimize absorption of the samples, and the spectral characteristics of MCX.

Collected patterns were refined by the Rietveld method using the FullProf program [35].

2.3 Optimization of the perovskitic structure and calculation of tilt angles

The theoretical basis of the software SPuDS is the bond valence model [36,37], that correlates the length of a bond to its strength, and hence the bond length to the valence. This correlation can be described as follows:

$$S_{ij} = exp\left(\frac{R_0 - R_{ij}}{B}\right) \qquad (2)$$

where S_{ij} is the bond valence associated to the interaction between the i^{th} and the j^{th} atom, R_{ij} is the *i-j* bond length, R_0 is a reference semi-empirical value based on a large number of experimentally determined *i-j* bond distances [38, 39], and B is a constant with typical value of 0.37 Å for oxides.

The valence of the i^{th} atom is then calculated by adding all the individual bond valence contributions S_{ij}:

$$V_i = \sum_j S_{ij} \qquad (3)$$

Perovskitic interatomic distances and tilt angles were calculated using SPuDS by entering space group, tilt system, both the identity and oxidation state of A and B cations, and temperature. SPuDS is based on the minimization of the Global Instability Index (GII), defined as:

$$GII = \left[\frac{\sum_{i=1}^{N} d_i^2}{N}\right]^{1/2} \qquad (4)$$

where d_i is the difference between the formal and the calculated bond valence sum for the i^{th} atom, and N is the number of atoms in the asymmetric unit. It can be calculated for any tilt system, and it is an indicator of its suitability for the description of the crystal structure: the lower is the GII value, the more probable is the adoption of the corresponding tilt system. At the end of the minimization process, the output provides optimized cell parameters, atomic positions and interatomic distances, as well as the GII value relative to all the possible tilt systems.

Moreover, SPuDS provides a calculation of the Goldschmidt t factor based on the bond valence model (t_{BV}), alternative to the one based on Shannon's ionic radii, making use of the temperature dependent ideal A-O and B-O interatomic distances in place of the sum of ionic radii in equation (1), under the assumption of 12 equal A-O and 6 equal B-O distances [32]. This choice is particularly advantageous mainly in two cases, namely when the 12-coordinated A radius is not available, and when a value of t at a temperature other than 298 K is necessary. The determination of t_{BV} at temperatures higher than 298 K implies the use of temperature dependent interatomic distances; in the framework of the bond valence model, this calculation is possible by using the thermal expansion factor of a bond, that can be expressed through the following equation:

$$dR/dT = k/2BG \quad (5)$$

where k is the Boltzmann constant, G the bond stretching force constant expressed in N/m, and B is the aforementioned constant used in Equation (2) [37]; G values are generally obtained from infrared and Raman spectroscopy [37], and are contained in the SPuDS database. Nevertheless, it is worth to underline that RE-O bond distances are generally known with a lower accuracy than atomic radii, and this fact has a direct consequence on the accuracy of the calculated t_{BV} value.

The octahedral tilt angle of perovskites optimized by SPuDS was calculated using the software TUBERS [32], starting from the oxygen atomic positions.

3. Results

3.1 Rietveld refinements

High temperature X-ray powder diffraction revealed that, in the chosen experimental conditions, the studied $LaREO_3$ oxides crystallize in the *Pnma* structure, represented in Figure 1 in comparison to the ideal structure belonging to the $Pm\bar{3}m$ space group. $LaErO_3$ and $LaTmO_3$ were found in the perovskitic form between 1173 and 1273 K, while $LaYbO_3$ between 1073 and 1273 K; at lower temperatures, samples are amorphous.

For each diffraction pattern, peak profiles were fitted using the pseudo-Voigt function, and the background by linear interpolation of a set of ~80 points taken from the spectrum. Starting values of lattice parameters and refinable atomic positions were derived from the Pearson's Crystal Structure Database [40]. In the last refinement cycles, the structural parameters (lattice parameters, oxygen coordinates and overall B factor), the scale factor, 5 peak parameters, and the background points were refined. Moreover, the zero position was refined too, and two asymmetry parameters were optimized to correct peak asymmetry. In Figure 2 the Rietveld refinement plot of $LaYbO_3$ at 1273 K is reported as a representative example. In Table 1 the refined lattice parameters, as well as R_B and χ^2 agreement factors, are reported for each sample; as expected, lattice parameters increase with increasing temperature.

It is noteworthy that, even if all the crystalline samples could be indexed and refined in the orthorhombic structure, not all the parameters optimized at the lowest temperature are equally reliable: those related to the oxygen positions are in fact affected by a higher uncertainty degree, since samples could have not still reached equilibrium. Moreover, both at 1173 and 1273 K, $LaErO_3$ contains a non-negligible amount of C phase, which decreases with increasing temperature (see Table 1). For these reasons, in the following discussion we take into account lattice parameters at all the temperatures, as they depend on the RE atom, while we consider only interatomic distances obtained at the highest temperatures [1273 K for RE ≡ Er and Tm; 1173-1273 K, for RE ≡ Yb], as they are strictly related to the oxygen positions.

3.2 Evaluation of the SPuDS optimization

The reliability of SPuDS to study the stability of perovskites characterized by a low *t* tolerance factor, such as the ones treated in this work, can be checked by comparing structural data obtained by Rietveld refinements to the ones optimized by SPuDS at the same temperature. A synopsis of experimental and calculated parameters, chosen for their significance in the subsequent discussion, is reported in Table 2.

It can be noticed that cell volumes are slightly underestimated by SPuDS, with a discrepancy between experimental and calculated values that ranges between 1.4% (for $LaTmO_3$) and 3.4% (for $LaErO_3$). This result is in agreement with the assessment of SPuDS accuracy in the determination of lattice parameters of perovskites belonging to the *Pnma* space group [32]; it is in fact stated that at low *t* values both the calculated *a* and *c* cell parameter are slightly lower than the experimental ones, giving rise to an underestimation of cell volumes.

BO_6 octahedra are forced by SPuDS to maintain a regular shape, i.e. the six B-O distances are fixed at equivalent values, and no oxygen displacements are allowed. The validity of this approximation was checked by analyzing the B-O distances obtained from our Rietveld refinements. Three pairs of B-O distances arise from the atomic arrangement, namely two different pairs of basal B-O1 distances (d_{bas}) and one of apical B-O2 distances (d_{apic}). The d_{apic}/d_{bas} ratio

ranges between 1.0456 ($LaYbO_3$ at 1073K) and 0.9782 ($LaErO_3$ at 1273K), while the d_{bas1}/d_{bas2} ranges between 1.0925 ($LaYbO_3$ at 1173K) and 1.0085 ($LaTmO_3$ at 1273K). These values, that correspond to a maximum percentage discrepancy of 4% between any B-O distance and the average one, allow to conclude that the constraint on BO_6 polyhedra is fully acceptable. Anyway, the small displacements of oxygen atoms surrounding the B atom are neglectable if compared to the greater compressibility and thermal expansivity of the AO_{12} polyhedra.

In the cubic ideal perovskite the coordination polyhedron around the A atom is a regular cubo-octahedron, characterized by twelve equivalent A-O distances; in the *Pnma* distortion they are replaced by four non equivalent A-O2 distances and four non equivalent pairs of A-O1 distances. When the structure is strongly distorted, such as in the case of interlanthanide perovskites, from the crystallographic point of view, the A coordination number is considered to be reduced to 8, resulting in a distorted square antiprism; nevertheless, when considering the A-O interaction, the contribution to the bond valence sum of all the 12 oxygen atoms is significant; indeed, the longest A-O distances are crucial in the evaluation of the phase stability, since if they exceed a certain threshold length, the perovskitic structure collapses in favor of a more stable atomic arrangement. In Figure 3 the regular AO_{12} polyhedron is sketched and compared to the distorted one; in the latter, dotted lines represent vertices joining atoms of the inner coordination sphere to the 4 atoms of the outer sphere.

The experimental longest La-O1 interatomic distance results to be in substantial agreement with the one calculated for $LaErO_3$ and $LaYbO_3$, with a maximum difference of ~5%; in the case of $LaTmO_3$, on the contrary, the calculated distance exceeds the experimental one by 9%. This non negligible discrepancy can be explained by taking into account the difference between values of the Goldschmidt t factor calculated from the Shannon ionic radii (t_{IR}) and from the bond valence method (t_{BV}). t_{BV} is generally slightly lower than t_{IR}; an analysis performed on a large number of ABO_3 perovskitic and non-perovskitic oxides [23] shows in fact that the correlation between t_{BV} and t_{IR} is described by the following equation:

$$t_{BV} = 1.015 t_{IR} - 0.015 \quad (6)$$

A lower value of t_{BV} with respect to t_{IR} is observed also in the case of interlanthanide perovskites, as observable in Figure 4, where t_{BV} and t_{IR}, calculated at room temperature, are reported as a function of the B ionic radius for a series of $LaREO_3$ mixed oxides (RE ≡ Gd-Lu). Moreover, the trends of t_{IR} and t_{BV} shown in Figure 4 point to a higher regularity of the former, due to the aforementioned lower accuracy of t_{BV} with respect to t_{IR} values. Despite the differences between the two trends, the sequence of both t_{BV} and t_{IR} values is expected to be increasing with decreasing the B radius; nevertheless, as evident from the trend of data included in the frame in Figure 4, relative to two of the compositions experimentally treated in this work, t_{BV} and t_{IR} of $LaTmO_3$ are remarkably different, and t_{BV} of $LaTmO_3$ is lower than t_{BV} of $LaErO_3$. This deviation from the expected sequence of t_{BV} values is quite unrealistic, since it implies longer RE-O distances for RE ≡ Tm than for RE ≡ Er, despite $r_{Tm} < r_{Er}$.

As a consequence, the discussion of the stability criterion of interlanthanide perovskites based on the structural optimization by the bond valence method, has to be carefully considered when dealing with mixed oxides containing Tm, even more if the Tm-containing mixed oxide is located close to the perovskitic phase boundary. Similarly, attention has to be paid when treating mixed oxides containing Dy, due to the unexpected high t_{BV} value (see Figure 4). In all other cases, the optimization process performed by SPuDS can be considered as highly reliable, and the results can be used to derive a stability criterion for interlanthanide perovskites.

4. Discussion

The stability range of interlanthanide perovskites ABO_3 as a function of temperature has been determined in a number of papers going back to the Seventies of last century [24,25,26,27,28], as well as in more recent articles of this research group [10,11]. Combined results of these investigations are reported in Figure 5, where the stability ranges of ten perovskites are shown as a function of t_{IR}; $CeYbO_3$ and $NdLuO_3$ do not appear in Figure 5, as for both compositions transition

temperatures are not available in the literature; moreover, due to the lack of experimental data, for $PrYbO_3$, $CeTmO_3$, $CeLuO_3$ and $PrLuO_3$, only the decomposition temperature (*i.e.* the upper temperature limit) and for $LaLuO_3$ only the formation temperature (*i.e.* the lower temperature limit), are shown. It can be noticed that with increasing t the formation temperature of the perovskitic phase decreases and the decomposition temperature increases, with a general expansion of the stability range. Phases resulting from the decomposition of the perovskitic structure are reported too, showing that perovskites with the lowest t values ($LaHoO_3$, $LaYO_3$, $CeTmO_3$) decompose into the monoclinic B form, the ones with intermediate t values ($LaErO_3$) decompose into the H form, while at the highest t they undergo at high temperature a transition towards the X form ($LaTmO_3$, $LaYbO_3$, $CeLuO_3$, $PrLuO_3$, $PrYbO_3$). This evidence can be explained considering that with increasing t the decomposition temperature rises, so that perovskites decompose into phases stable at progressively higher temperature, i.e. following the sequence B→H→X [41]. As observable in Figure 5, some perovskitic compositions ($LaHoO_3$, $LaYO_3$ and $LaErO_3$) derive from the decomposition of the cubic C phase, typical of rare earth sesquioxides and mixed oxides at low temperature. As a phase transition takes place when the phases in equilibrium have the same Gibbs free energy, the amplitude of the perovskitic range has to be studied by analyzing structural features not only of the perovskite, but also of the low and high temperature phases.

4.1 Relationships between perovskite and other structural forms of rare earth oxides

The low temperature phase C is the cubic form typical of sesquioxides of the smallest rare earths, belonging to the $Ia\bar{3}$ space group. It can be considered as formally derived from the fluoritic structure typical for example of CeO_2 by removal of one fourth O atoms; thus, rare earth atoms result to be located in two distinct atomic sites, namely the 24*d* in (x, 0, ¼) and the 8*a* in (0, 0, 0), forming two different corner- and edge-sharing distorted octahedra. Thus, the C→perovskite transition occurs with a coordination change for rare earth atoms from two octahedra (C.N. 6) to an A-centred distorted square antiprism (C.N. 8) and a B-centred octahedron, *i.e.* with a mean coordination number increase, as expected with increasing temperature. The C→perovskite

transition occurs along with an order increase, as cations are randomly distributed over both atomic sites in the C structure, while they occupy non-interchangeable atomic positions in the perovskite, due to the described size constraints. Nevertheless, due to the low temperatures involved, the dimensional issue prevails over the entropic one.

Regarding the high temperature phases, the H (hexagonal) and X (cubic) forms are not well known, since they are stable only at high temperature; both of them are formed by octahedra, strongly distorted in the case of the H structure [42]. The B form, on the contrary, is the monoclinic structure typical of rare earth sesquioxides (isotypic with Sm_2O_3), belonging to the $C\,2/m$ space group. The perovskite→B transition promotes an energy gain in terms of Gibbs free energy, due to a substantial increase in the entropic contribution. While in fact, as aforementioned, cations occupy well defined positions in the perovskitic structure, they can randomly distribute over three cationic sites located in $4i$ (x, 0, z) in B. Around them three coordination polyhedra can be built, namely two monocapped trigonal prisms, and an octahedron; for all the cation-oxygen interatomic distances, in the case of monoclinic $LaYO_3$ [25] minimum and maximum values lie within the range 2.266-2.388 Å, and 2.644-2.797 Å, respectively. The narrowness of these intervals allows to conclude that no preferential sites are present in this structure, and cations randomly distribute over the three sites, as reported both in [25] for $LaYO_3$ and in [43] for $La_{1.3}Y_{0.7}O_3$. A similar scenario can be hypothesized for the H and X structures, since a complete miscibility of rare earth sesquioxides has been observed in several RE_2O_3-RE'_2O_3 mixed systems at high temperature [42]; nevertheless, caution must be used due to the limited knowledge of the cited structures.

Therefore, even if interesting, the previous discussion has a qualitative character, due to two main shortcomings, namely: a) the temperature range of the C phase, often too low to allow a sufficient crystallinity degree of samples, and hence the obtainment of reliable atomic positions; b) the lacking structural information about the H and X phases, because of the impossibility to obtain them at room temperature by quenching. For these reasons, the issue related to the stability range of

interlanthanide perovskites can be better dealt with by considering the stability factors acting on perovskites themselves.

The Goldschmidt t factor is generally considered as the stability indicator of the perovskitic phase, but when the temperature dependence is studied, it is not sufficient to explain the extent of the stability range; stability can be more conveniently discussed in terms of factors ascribable to enthalpic and entropic contributions to the Gibbs free energy of the phase. A confirmation of the inability of the t factor to describe the temperature dependence of the perovskitic stability comes from the calculation of t_{BV} in perovskites characterized by $t<1$, that provides indefinitely increasing values with rising temperature; this result would point to a stability increase with temperature, so contradicting the experimental evidence. The reason of this behaviour lies in the unequal elongation of A-O and B-O distances with increasing temperature, due to the higher value of the force constant G in Equation (5) for shorter bonds, that produces an increase in the ratio $\frac{d_{A-O}}{d_{B-O}}$ with increasing temperature, and thus in the t_{BV} value. This inconsistency can be overcome if the purely geometric t factor is considered in the wider context of the different energetic contributions to phase stability, *i.e.* if factors of enthalpic and entropic nature are taken into account.

The two effects of the t increase on the perovskitic stability extent, namely a lower formation temperature and a higher decomposition temperature, can be more conveniently separately analyzed, as it can be hypothesized that the former is ascribable to the enthalpic contribution to the free energy, and the latter to the entropic factor.

4.2 Effect of t on the perovskitic lower temperature limit

A qualitative evaluation of the enthalpic contribution can be performed by analyzing interatomic distances sensitive to the variation of the tilt angle, with the aim to derive a trend of the energetic gain related to the formation of a certain bond. Since BO_6 octahedra are restricted by SPuDS to maintain a regular shape, the variation of A-O distances within the A coordination sphere are considered, in order to discuss the position of the lower perovskitic boundary. Among the twelve

different A-O interatomic distances, the longest one has been analyzed in more detail, since its length at the perovskitic boundary can be correlated to the perovskitic formation temperature. This choice does not mean that the cited distance is responsible for the entire enthalpic contribution, but that it can be considered as an indicator accounting for the enthalpic factor originating from the whole structure.

For each perovskite, t_{BV} decreases with decreasing temperature, meaning that the structure becomes more and more distorted to preserve the perovskitic form. The increasing distortion consists in an increasing tilting of the BO_6 octahedra, as confirmed by the tilt angle values reported in Table 3: they are calculated at the lower temperature limit and coupled to t_{BV} calculated at the same temperature. The effect of the increasing BO_6 octahedral tilting is a progressive reduction of the A-centred polyhedral volume; in interlanthanide perovskites, characterized by a low value of t, due to the small size of the A atom, the reduction of the space available for A favours the phase stability. A further effect of an increased octahedral tilting is the displacement of oxygen atoms coordinating A, with the subsequent creation of an irregular polyhedron, characterized by strongly elongated and shortened A-O distances with respect to the ideal cubic case. Thus, the position of the perovskitic lower boundary can be studied taking into account the longest A-O distance: in these terms the formation temperature can be considered as the lowest temperature that guarantees a bonding character to A-O interactions; below this limit, the longest A-O distance becomes too long to ensure bonding, and atoms prefer an energetically more convenient arrangement.

To compare values deriving from different A atoms, the longest A-O distance provided by SPuDS for each perovskite at the observed lower temperature limit, has been normalized dividing it by the ideal A-O distance $(A-O)_{id}$ calculated at the same temperature; the so defined ratio $(A-O)_{max}/(A-O)_{id}$ is hereafter named d_{norm}. $(A-O)_{id}$ is the R_0 parameter in Equation (2) relative to the A-O pair: it is empirically determined over a large number of A-O experimental bond distances; it depends on temperature, and it is defined as the A-O distance that produces a bond valence of the A-O interaction equal to 1 (see equation 2). Room temperature values of $(A-O)_{id}$

of interest for this work are reported in [38]; high temperature values were obtained by applying a thermal expansion coefficient of $4.5*10^{-5}$ Å/K. In Table 3 d_{norm} values are reported for $LaREO_3$ perovskites (RE ≡ Y, Ho-Lu). It can be noticed that the lower is t_{BV}, the higher are the tilt angle and d_{norm}, thus confirming the strict relation between tilt angle and distortion of the A-centred polyhedron. A value of d_{norm} around 1.96, corresponding to a bond valence of 0.0031 valence units (v.u.), can be then considered as the upper limit of the normalized longest A-O distance that guarantees the stability of the perovskitic structure. Our conclusions are supported by the experimental results recently obtained by Qi *et al.* [13], who measured the formation enthalpies at room temperature of $LaREO_3$ perovskites (RE ≡ Ho-Yb) and found values that become increasingly negative with increasing *t*.

4.3 Effect of t on the perovskitic upper temperature limit

While the perovskitic lower temperature limit is related to a contribution of enthalpic nature to the phase free energy, the upper limit can be regarded as strictly connected to the entropic decrease associated to the formation of a more and more regular coordination sphere around A, occurring with increasing temperature. Along with the atomic thermal vibration, also the order degree of the phase contributes in fact to the entropic factor, and the high temperature perovskitic boundary is located where the thermal- and the displacement-related factors concurring to entropy, give rise to a Gibbs free energy of the perovskitic phase equal to the one of another atomic arrangement.

As previously described, the value of the tilt angle determines the distortion degree of the A-centred polyhedron; in this sense, it is an indicator both of the enthalpic and the entropic contribution to the perovskitic free energy; its decrease with increasing temperature accounts for an entropic destabilization of the perovskitic phase, since it is a measure of the increased regularity of the polyhedron. It can be expected that the higher is the enthalpic gain at a given temperature (*i.e.* the higher is *t* and the more regular is the A-centred polyhedron), the higher is the temperature where the destabilizing entropic contribution becomes crucial; as tilt angles decrease with increasing temperature, it is expected that tilt angles calculated at the decomposition temperature

show decreasing values with increasing t. This behaviour is indeed observed, as evident in Figure 6. This means that high t values correspond to high decomposition temperatures; since at the same they are responsible of low formation temperatures, it can be concluded that a correlation exists between the t value and the perovskitic temperature range.

4.4 Validation of the proposed criterion

The upper limit of d_{norm} and the minimum tilt angle can be then taken as the key parameters describing the low and high temperature boundaries of the perovskitic phase, respectively. Based on the described criteria, the formability of other interlanthanide perovskites can thus be predicted. If data reported in Figure 6 are interpolated by linear regression, the equation of the regression line can be used to extrapolate a value for the minimum tilt angle of other equimolar interlanthanide mixed oxides in the perovskitic form. By introducing the so obtained minimum tilt angle into SPuDS, it is possible to obtain the corresponding temperature, that acts as the hypothetic decomposition temperature. The value of the longest A-O distance at that temperature is then used to calculate d_{norm}. By comparing the so obtained d_{norm} with the limit value of 1.96, it is therefore possible to predict the formability and the possible temperature range of the interlanthanide perovskite under study. If $d_{norm} \geq 1.96$, no perovskitic range exists, since the lower temperature limit (located at $d_{norm}=1.96$) is higher than the upper limit; if on the contrary, $d_{norm}<1.96$, a perovskitic range is expected to exist, and its extent can be calculated.

The proposed stability criterion was checked by evaluating the formability of eleven equimolar interlanthanide mixed oxides that are reported as non perovskitic [8]; they are characterized by t values just slightly lower than the ones of the perovskites studied in this work. Among them, $NdLuO_3$ is included too; its existence is in fact quite doubtful, as it has been obtained in a polyphasic form by Berndt *et al.* [29] by solid state reaction of coprecipitated mixed hydroxides, while more recently it could not be prepared by Ito *et al.* [8] by the same method. The decomposition temperatures of the hypothetic perovskites were calculated by extrapolating the minimum tilt angle, as previously described; the maximum A-O distance at the decomposition

temperature was calculated too, and the resulting values are reported in Table 4. A very good agreement between our data and the experimental results reported in the literature can be noticed.

Two different cases are recognizable. a) For the great majority of compositions ($CeDyO_3$, $PrTmO_3$, $PrErO_3$, $PrHoO_3$, $PrDyO_3$, $NdLuO_3$, $NdYbO_3$, $NdDyO_3$), the calculated d_{norm} is so high with respect to the reported limit of 1.96, and the decomposition temperature is so low, that it is not possible to hypothesize the existence of a perovskitic temperature range. $NdLuO_3$ belongs to this group, so that our data confirm the conclusion of Berndt *et al.* [29], who state that $NdLuO_3$ is not thermodynamically stable. b) For the other compositions ($LaDyO_3$, $CeErO_3$, $CeHoO_3$) the calculated d_{norm} value is close to 1.96, but considering the very low calculated decomposition temperatures of many of them, only for $CeErO_3$ it could be possible to suppose the existence of a narrow perovskitic range, however until now not experimentally observed.

The deduced stability criterion based on the geometrical limits to the phase stability can be then considered reliable for perovskites characterized by *t* values close to the lower limit. It can provide hints for the possible obtainment in the perovskitic form, by using the proper synthetic techniques, of equimolar mixed oxides until now observed only in other structural forms.

5 Conclusions

Literature data regarding interlanthanide perovskites have been assessed with the aim to study the existence range of the cited oxides as a function of temperature. A stability criterion has been derived from geometrical issues affecting the enthalpic and the entropic contribution to the Gibbs free energy of the perovskitic phase, and verified by applying it to non-perovskitic equimolar mixed oxides with *t* values close to the ones of interlanthanide perovkites. Ideal interatomic distances and tilt angles were calculated by the bond valence method; the reliability of the SPuDS software was checked by comparing some selected structural parameters experimentally obtained by high temperature synchrotron X-ray diffraction performed on $LaErO_3$, $LaTmO_3$ and $LaYbO_3$ at 1173 and

1273 K, to the ones optimized at the same temperature by the software; some critical points regarding the calculation of t_{BV} and the evaluation of cell volumes were highlighted too.

Acknowledgements

The Elettra Synchrotron Radiation Facility is acknowledged for the provision of beam time. Authors are grateful to Dr. Jasper Plaisier for assistance in performing measurements at the MCX beamline.

References

[1] T. Norby, Solid State Ionics 125 (1999) 1-11.

[2] Y. Okuyama, T. Kozai, S. Ikeda, M. Matsuka, T. Sakai, H. Matsumoto, Electrochim. Acta 125 (2014) 443-449.

[3] Y. Okuyama, T. Kozai, T. Sakai, M. Matsuka, H. Matsumoto, Electrochim. Acta 95 (2013) 54-59.

[4] E. Ruiz-Trejo, M.S. Islam, J.A. Kilner, Solid State Ionics 123 (1999) 121-129.

[5] W. T. Su, L. Yan, B. Li, Appl. Surf. Sci. 257 (2011) 2526-2530.

[6] M. Olyaei, B. Gunnar Malm, P.E. Hellström, M. Östling, Solid-State Electron. 78 (2012) 51-55.

[7] A. Martinelli, R. Masini, C. Artini, G.A. Costa, L. Keller, J. Phys.: Condens. Matter 25 (2013) 426005 1-7.

[8] A. Martinelli, C. Artini, L. Keller, submitted to J. Phys.: Condens. Matter

[9] K. Ito, K. Tezuka, Y. Hinatsu, J. Solid State Chem. 157 (2001) 173-179.

[10] C. Artini, G.A. Costa, M.M. Carnasciali, R. Masini, J. Alloy Compd. 494 (2010) 336-339.

[11] C. Artini, G.A. Costa, R. Masini, J. Therm. Anal. Calorim. 103 (2011) 17-21.

[12] M. Bharathy, A.H. Fox, S.J. Mugavero, H. C. zur Loye, Solid State Sci. 11 (2009) 651-654.

[13] J. Qi, X. Guo, A. Mielewczyk-Gryn, A. Navrotsky, J. Solid State Chem. 227 (2015) 150-154.

[14] P.M. Woodward, Acta Cryst. B 53 (1997) 32-43.

[15] P.M. Woodward, Acta Cryst. B 53 (1997) 44-66.

[16] V.B. Shirokov, V.I. Torgashev, Crystallogr. Rep. 49 (2004) 20-28.

[17] A.M. Glazer, Acta Cryst. B 28 (1972) 3384-3392.

[18] K.S. Aleksandrov, Kristallografiya 21 (1976) 249-255.

[19] V.M. Goldschmidt, Naturwissenschaften, 14 (1926) 477-485.

[20] R.D. Shannon, Acta Cryst. A 32 (1976) 751-767.

[21] S. J. Schneider, R. S. Roth, J. Res. Nat. Bur. Stand. A 64 (1960) 317-332.

[22] C. A. Randall, A. S. Bhalla, T. R. Shrout, L. E. Cross, J. Mater. Res. 5 (1990) 829-834.

[23] H. Zhang, N. Li, K. Li, D. Xue, Acta Cryst. B 63 (2007) 812-818.

[24] A. Rouanet, J. Coutures, M. Foex, J. Solid State Chem. 4 (1972) 219-222.

[25] J. Coutures, M. Foex, J. Solid State Chem. 11 (1974) 294-300.

[26] U. Berndt, D. Maier, C. Keller, J. Solid State Chem. 13 (1975) 131-135.

[27] J. Coutures, A. Rouanet, R. Verges, M. Foex, J. Solid State Chem. 17 (1976) 171-182.

[28] J. Coutures, J.P. Coutures, J. Solid State Chem. 19 (1976) 29-33.

[29] U. Berndt, D. Maier, C. Keller, J. Solid State Chem. 16 (1976) 189-195.

[30] J. Coutures, F. Sibieude, M. Foex, J. Solid State Chem. 17 (1976) 377-384.

[31] M. Foex, J.P. Traverse, Rev. Int. Hautes Temper. Refract. 3 (1966) 429-453.

[32] M.W. Lufaso, P.M. Woodward, Acta Cryst. B 57 (2001) 725-738.

[33] C. Artini, G.A. Costa, M. Pani, A. Lausi, J. Plaisier, J. Solid State Chem. 190 (2012) 24-28.

[34] C. Artini, M. Pani, A. Lausi, R. Masini, G.A. Costa, Inorg. Chem. 53 (2014) 10140-10149.

[35] J. Rodriguez-Carvajal, Phys. B 192 (1993) 55-69.

[36] I.D. Brown, Chem. Soc. Rev. 7 (1978) 359-376.

[37] I.D. Brown, The chemical bond in inorganic chemistry – The bond valence model, Oxford University Press, New York, 2002.

[38] I.D. Brown, D. Altermatt, Acta Cryst. B 41 (1985) 244-247.

[39] http://www.iucr.org/__data/assets/file/0006/81087/bvparm2013.cif.

[40] P. Villars, K. Cenzual, Pearson's Crystal Data - Crystal Structure Database for Inorganic Compounds, Release 2012/13, ASM International, Materials Park, Ohio, USA.

[41] L. Eyring, in: K.A. Gschneidner Jr., L. Eyring (Eds.) Handbook on the Physics and Chemistry of Rare Earths, North Holland, 1979, 3, pp. 337-399.

[42] M. Zinkevich, Progr. Mater. Sci. 52 (2007) 597-647.

[43] L.M. Lopato, B.S. Nigmanov, A.V. Shevchenko, Z.A. Zaitseva, Inorg. Mater. 22 (1986) 678-681.

Figure captions

Figure 1 – Representation of the ideal cubic ($Pm\bar{3}m$) and distorted orthorhombic ($Pnma$) structures.

Figure 2 – Plot of Rietveld refinement of $LaYbO_3$ at 1273 K. The red and black lines are the experimental and the calculated diffractogram, respectively; the lower line is the difference curve; vertical bars indicate the calculated positions of Bragg peaks; hkl indexes of the main peaks are reported too.

Figure 3 – The AO_{12} polyhedron in the ideal cubic ($Pm\bar{3}m$) structure (a) and in the distorted ($Pnma$) one (b).

Figure 4 – Trend of t_{IR} and t_{BV} values for $LaREO_3$ mixed oxides as a function of the RE ionic radius. In the frame values relative to $LaTmO_3$ and $LaErO_3$ are included to highlight the unexpected low value of t_{BV} for $LaTmO_3$. In order to allow a direct comparison, t_{IR} and t_{BV} are calculated at room temperature.

Figure 5 – Stability range of interlanthanide perovskites ABO_3 as a function of t_{IR}. For $PrYbO_3$, $PrLuO_3$, $CeLuO_3$ and $CeTmO_3$, only the upper temperature limit is available, while for $LaLuO_3$ only the lower temperature limit is known. In case of unavailability of the A ionic radius, t_{IR} was calculated from t_{BV} through equation (6). P: perovskite (sp. gr. $Pnma$); C: cubic (sp. gr. $Ia\bar{3}$); B: monoclinic (sp. gr. $C\,2/m$); H and X: high temperature structures. The green dashed line indicates the stability range of the perovskitic phase.

Figure 6 – Trend of the tilt angle at the decomposition temperature as a function of t_{IR}. The regression line is shown too.

Figure 1
Click here to download high resolution image

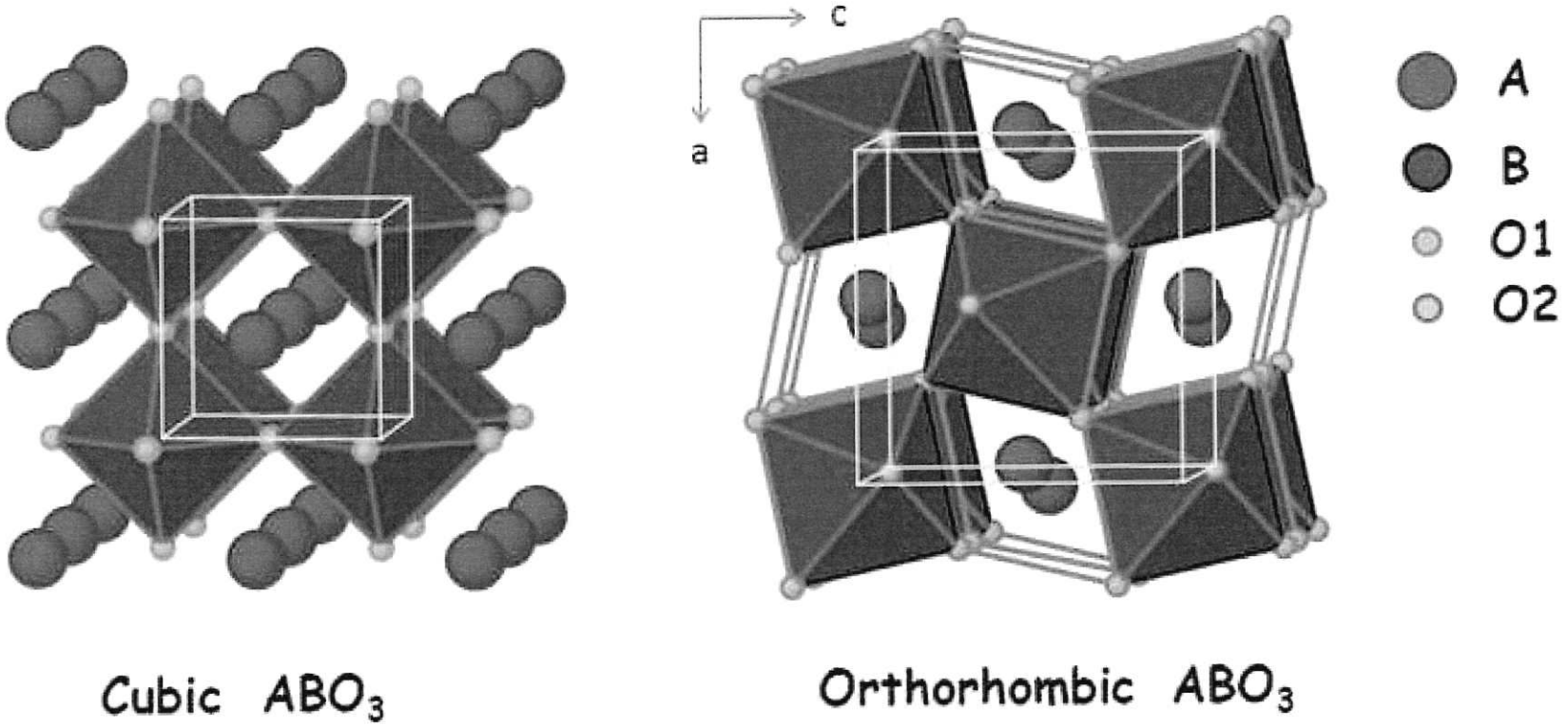

Figure 2
Click here to download high resolution image

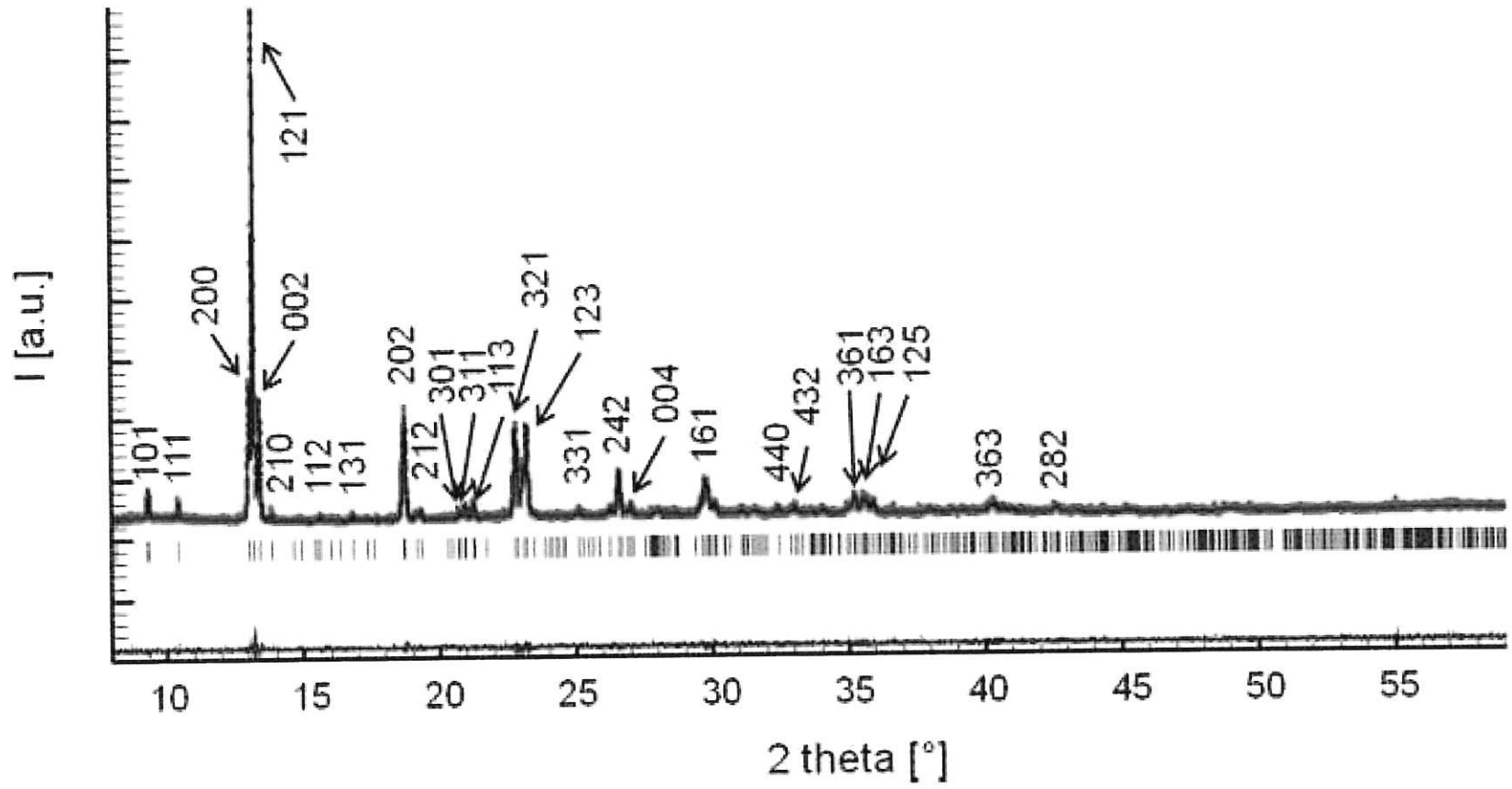

Figure 3
Click here to download high resolution image

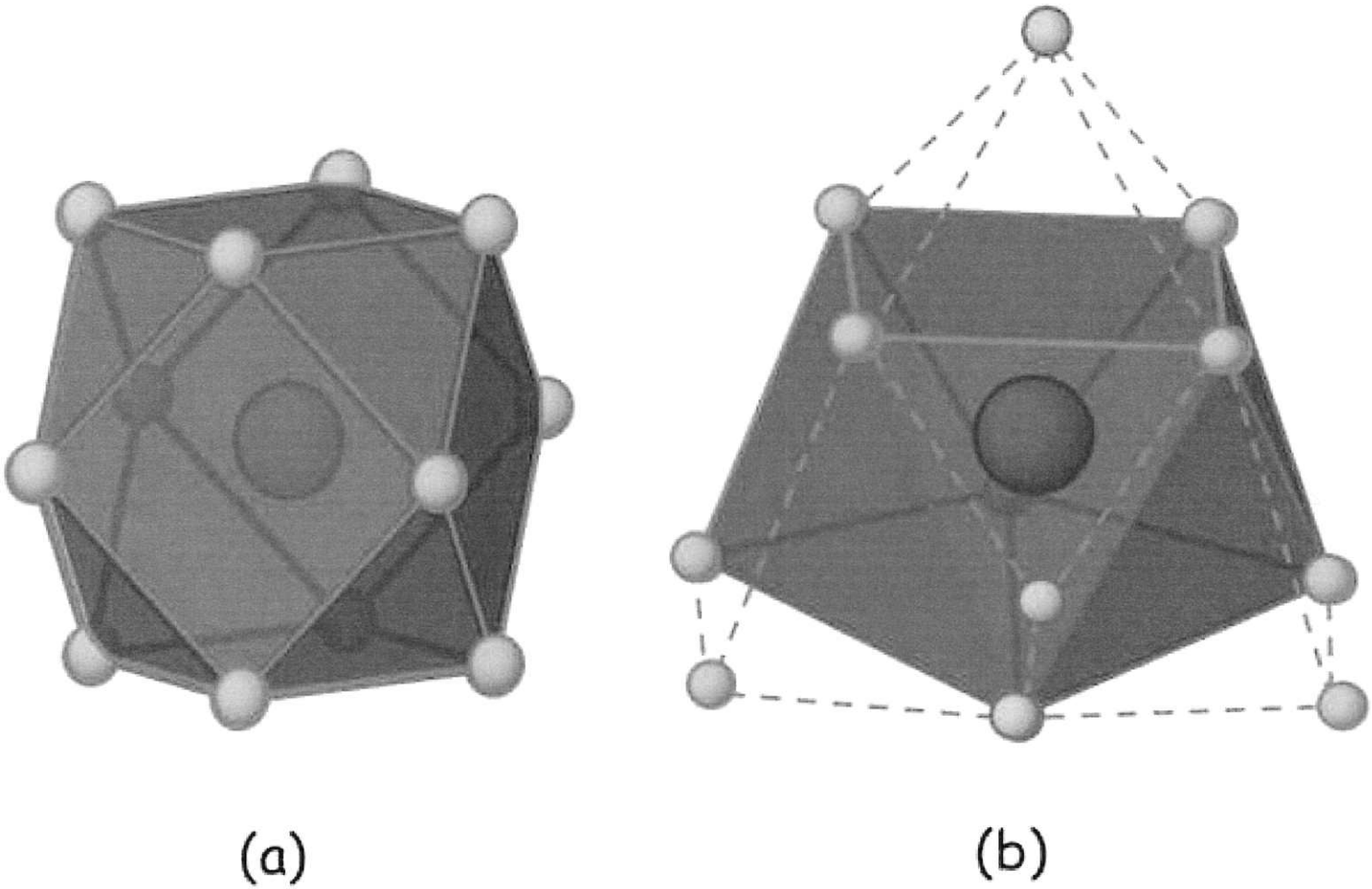

Figure 4
Click here to download high resolution image

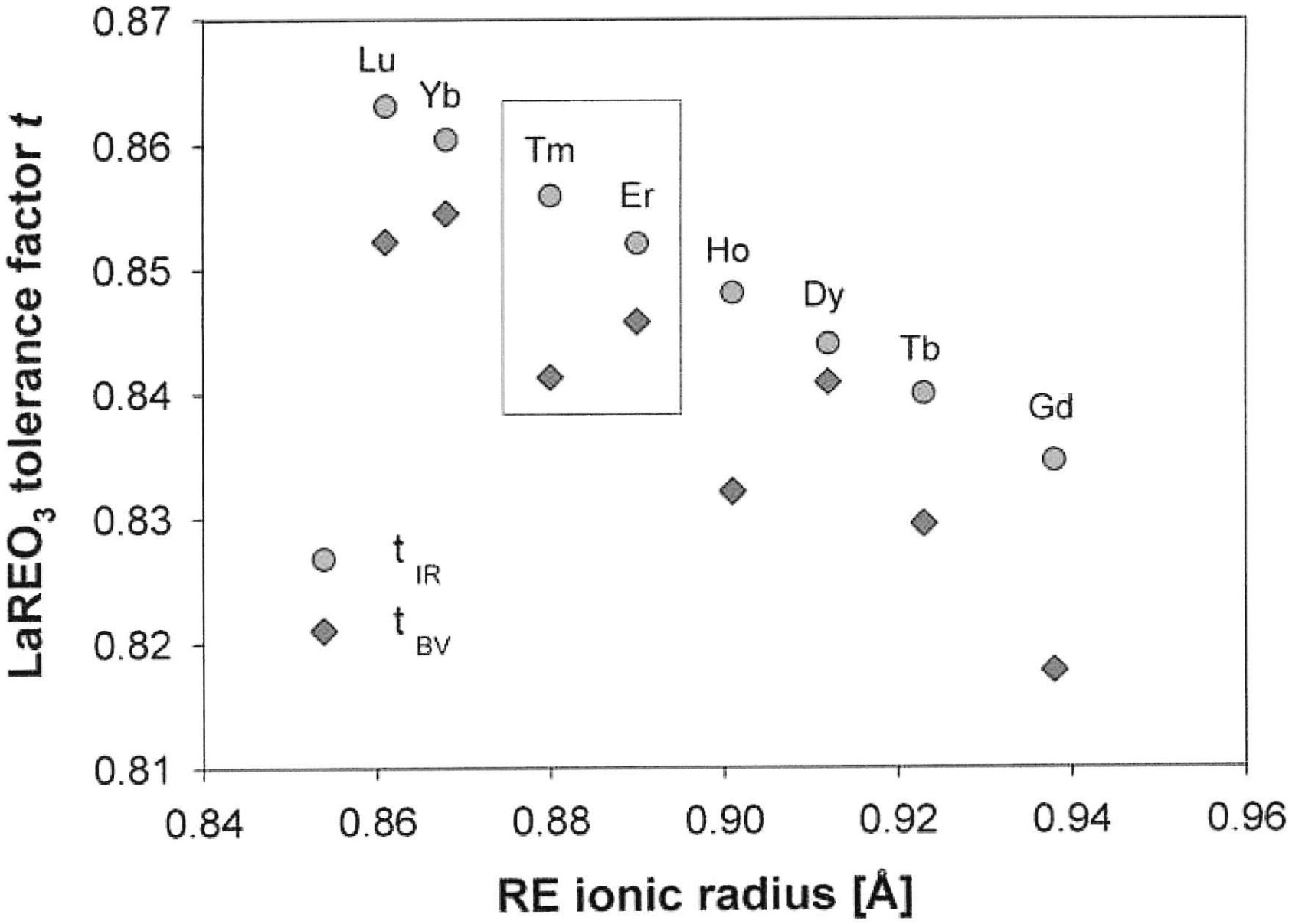

Figure 5
Click here to download high resolution image

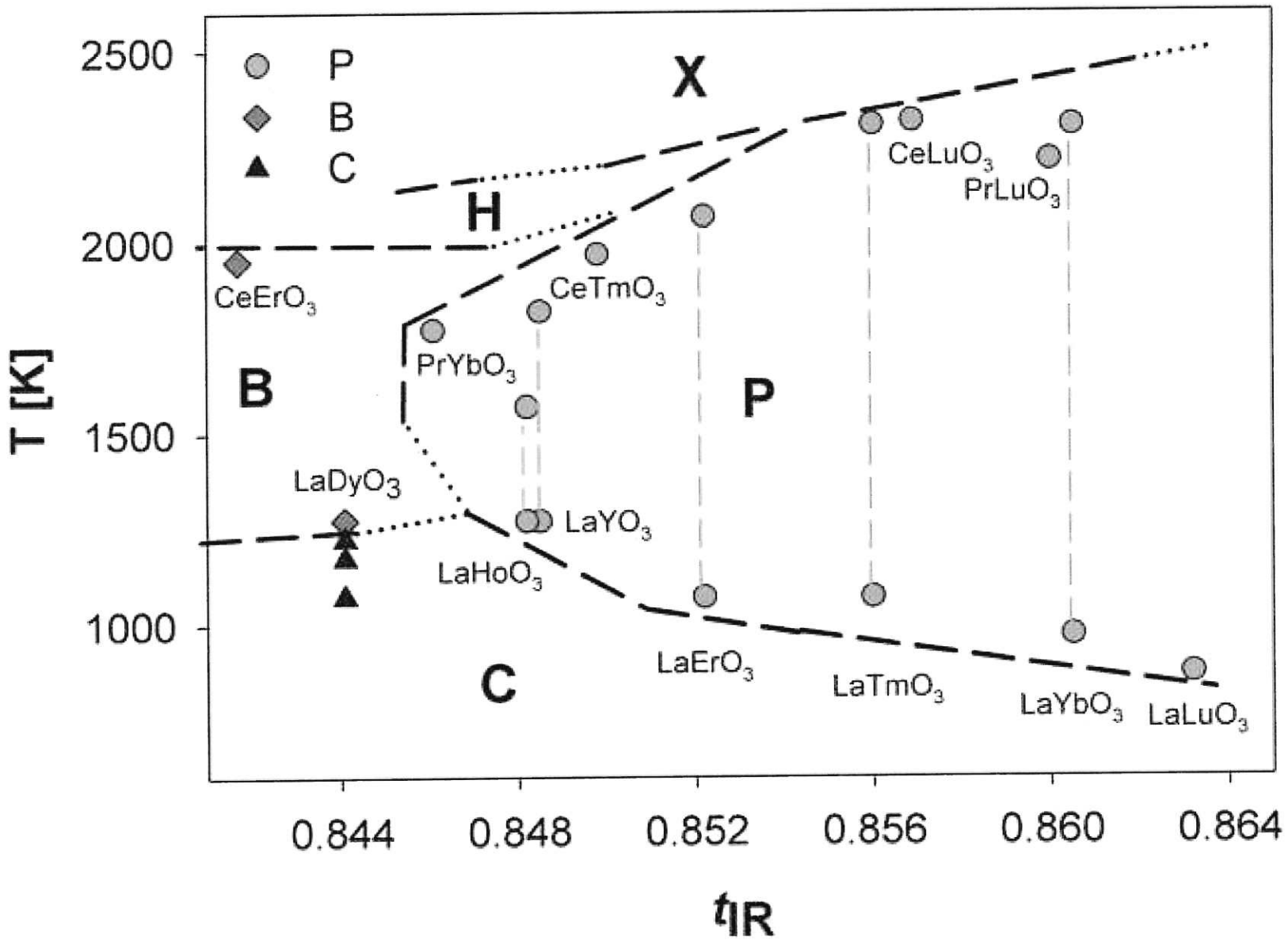

Figure 6
Click here to download high resolution image

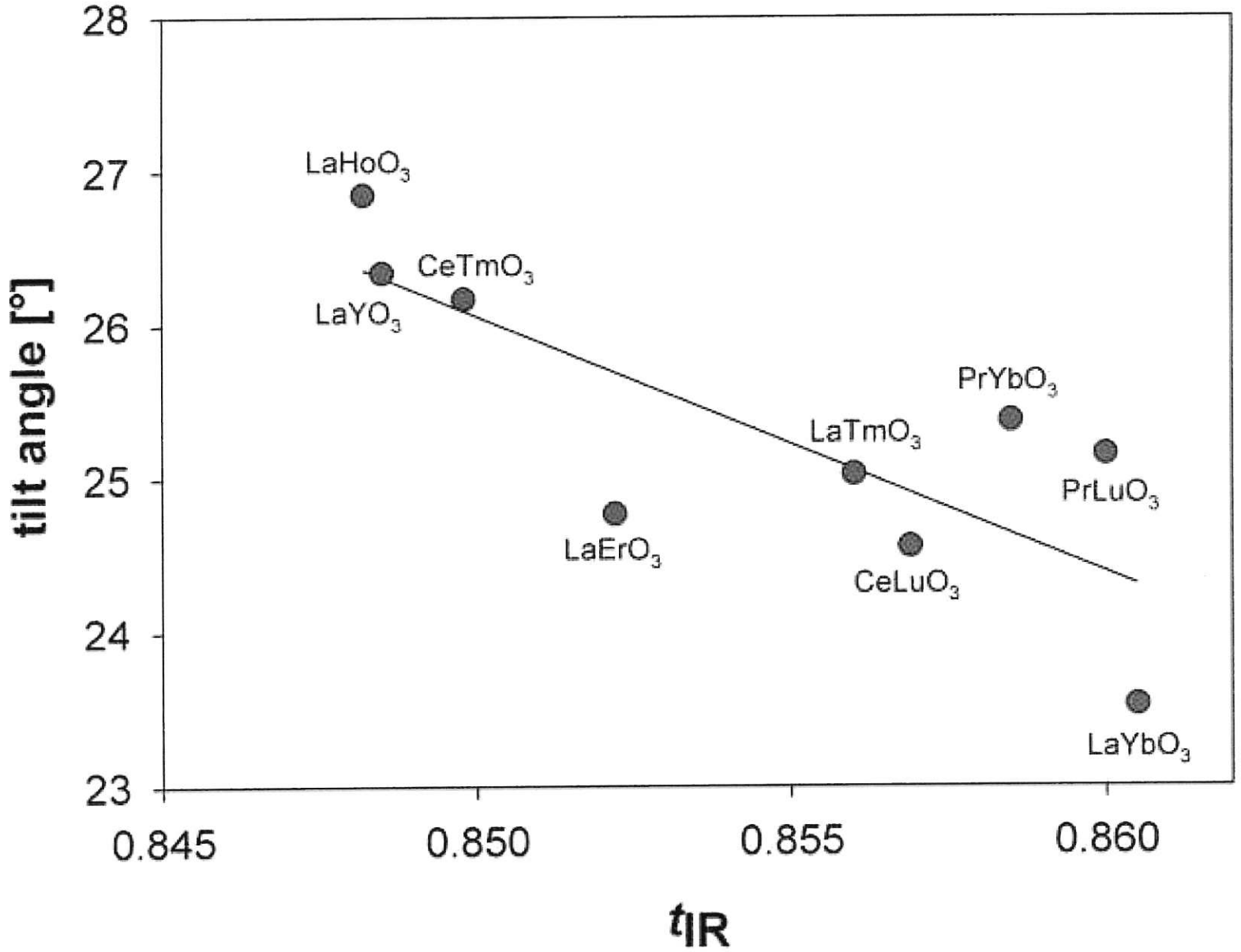

Table 1

Table 1 – High temperature lattice parameters and agreement factors of interlanthanide perovskites.

Sample	Phases[a)]	T [K]	a [Å]	b [Å]	c [Å]	R_B	χ^2
$LaErO_3$	80 wt.% C +20 wt.% P	1173	6.1184(2)	8.5477(2)	5.9183(2)	17.2	2.46
	83 wt.% P +17 wt.% C	1273	6.11045(8)	8.5523(1)	5.93016(7)	7.47	1.78
$LaTmO_3$	P	1173	6.08113(9)	8.5112(1)	5.90548(8)	6.80	1.61
	P	1273	6.08510(9)	8.5171(1)	5.91191(7)	8.11	1.55
$LaYbO_3$	P	1073	6.06034(8)	8.4814(1)	5.88511(7)	4.83	1.52
	P	1173	6.06403(7)	8.4865(1)	5.89209(6)	13.7	1.99
	P	1273	6.06577(5)	8.49035(7)	5.89721(5)	5.93	1.51

[a)] C ≡ C phase; P ≡ perovskite

Table 2

Table 2 – Comparison between experimental (from Rietveld refinements) and calculated (from SPuDS software) cell volumes and longest La-O distances. Goldschmidt *t* factors calculated both from Shannon's ionic radii (t_{IR}) and from the bond valence method (t_{BV}) are indicated too; t_{IR} is referred to room temperature.

Sample	T [K]	t_{BV}	t_{IR}	Cell Volume [Å^3]		Longest La-O distance [Å]	
				Exp.	Calc.	Exp.	Calc.
$LaErO_3$	1173	0.8533	0.8522	309.52(3)	298.86	-	-
	1273	0.8541		309.90(1)	299.95	4.054(8)	4.2241
$LaTmO_3$	1173	0.8488	0.8560	305.65(1)	300.97	-	-
	1273	0.8496		306.40(1)	302.14	3.897(9)	4.2656
$LaYbO_3$	1073	0.8612	0.8605	302.49(1)	293.46	3.936(7)	4.1488
	1173	0.8621		303.22(1)	294.57	3.959(6)	4.1477
	1273	0.8629		303.709(7)	295.69	3.900(6)	4.1467

Table 3

Table 3 – Goldschmidt factor t_{BV}, tilt angle and normalized longest A-O distance $d_{norm} = {d_{(A-O)max}}/{d_{(A-O)id}}$ for $LaREO_3$ perovskites (RE≡Y, Ho-Lu) calculated at the formation temperature.

Composition	**Formation temperature [K]**	t_{BV}	**Tilt angle**	d_{norm}
$LaHoO_3$	1273	0.8404	27.18	1.962
$LaYO_3$	1273	0.8426	26.93	1.954
$LaTmO_3$	1073	0.8479	26.34	1.933
$LaErO_3$	1073	0.8524	25.83	1.915
$LaLuO_3$	873	0.8572	25.31	1.897
$LaYbO_3$	973	0.8604	24.94	1.884

Table 4

Table 4 – Calculated values of decomposition temperature T_d and $d_{norm} = {}^{d_{(A-O)max}}/_{d_{(A-O)id}}$ for eleven non perovskitic interlanthanide mixed oxides.

Composition	t_{IR}	T_d [K]	d_{norm}
$LaDyO_3$	0.8441	463	1.958
$CeErO_3$	0.8461	983	1.948
$CeHoO_3$	0.8420	1793	1.968
$CeDyO_3$	0.8380	243	1.998
$PrTmO_3$	0.8335	<100	-
$PrErO_3$	0.8360	<100	-
$PrHoO_3$	0.8316	633	2.033
$PrDyO_3$	0.8357	333	2.015
$NdLuO_3$	0.8350	243	2.030
$NdYbO_3$	0.8324	<100	-
$NdDyO_3$	0.8166	<100	-

- The stability of interlanthanide perovskites has been investigated.
- Perovskitic structures were optimized by the bond valence method using SPuDS.
- The reliability of SPuDS was checked by comparing experimental and calculated data.
- A stability criterion was deduced by studying the geometrical limits of the phase.
- The criterion was verified applying it to non-perovskitic interlanthanide oxides.

Graphical Abstract